Scientific Reports

https://doi.org/10.1038/s41598-026-50597-w

Article in Press

Permittivity evaluation of electrically thin low-loss materials by using a generalized free-space model without any formal calibration

Received: 6 February 2026

Accepted: 22 April 2026

Published online: 23 May 2026

Cite this article as: Hasar U.C., Korkmaz H. & Kaya Y. Permittivity evaluation of electrically thin low-loss materials by using a generalized free-space model without any formal calibration. *Sci Rep* (2026). https://doi.org/10.1038/s41598-026-50597-w

Ugur C. Hasar, Huseyin Korkmaz & Yunus Kaya

We are providing an unedited version of this manuscript to give early access to its findings. Before final publication, the manuscript will undergo further editing. Please note there may be errors present which affect the content, and all legal disclaimers apply.

If this paper is publishing under a Transparent Peer Review model then Peer Review reports will publish with the final article.

ARTICLE IN PRESS

© The Author(s) 2026. **Open Access** This article is licensed under a Creative Commons Attribution 4.0 International License, which permits use, sharing, adaptation, distribution and reproduction in any medium or format, as long as you give appropriate credit to the original author(s) and the source, provide a link to the Creative Commons licence, and indicate if changes were made. The images or other third party material in this article are included in the article's Creative Commons licence, unless indicated otherwise in a credit line to the material. If material is not included in the article's Creative Commons licence and your intended use is not permitted by statutory regulation or exceeds the permitted use, you will need to obtain permission directly from the copyright holder. To view a copy of this licence, visit http://creativecommons.org/licenses/by/4.0/.

ARTICLE IN PRESS

Permittivity Evaluation of Electrically Thin Low-Loss Materials by Using a Generalized Free-Space Model Without Any Formal Calibration

Ugur C. Hasar[*1,2], **Huseyin Korkmaz**[2,3], **and Yunus Kaya**[4]

[1]Gaziantep University, Department of Electrical and Electronics Engineering, Gaziantep, 27310, Türkiye
[2]Gaziantep University, Applied Electromagnetics Research Laboratory (Aer-Lab), Gaziantep, 27310, Türkiye[**]
[3]Kilis 7 Aralık University, Department of Electrical and Electronics Engineering, Kilis 79000, Türkiye
[4]Bayburt University, Department of Electronics and Automation, Bayburt, 69010 Türkiye
[*]uchasar@gantep.edu.tr
[**]https://aer-lab.gantep.edu.tr

ABSTRACT

A general free-space model based on reflection and transmission measurements is proposed for accurate permittivity determination of low-loss and electrically thin ($W < \lambda/4$ where W is the sample thickness and λ is the wavelength) samples. Unlike previous free-space methods studied in the literature, the proposed new model generalizes previous free-space models by considering the case that transmitting and receiving antenna regions have different reflection and transmission properties. Such a model, valid at any frequency or over the entire frequency band, considers different antenna characteristics or different cable connections in addition to unequal and non-zero reflection properties due to impedance mismatches and ringing effects between antennas and the sample. An objective function constructed on this model is derived. This function is shown to be free-from error network terms of transmitting and receiving antenna regions and not dependent on reference-plane transformation factors. The effect of sample misalignment is considered to evaluate its effect on permittivity determination by the proposed extraction method. Free-space measurements at X-band ($8.2 - 12.4$ GHz) of low-loss Rogers 4350B sample ($W \approx 1.52$ mm) and FR-4 sample ($W \approx 1.60$ mm) were then carried out to validate our method.

ARTICLE IN PRESS

1 Introduction

Microwave electromagnetic characterization constitutes one of the building blocks of microwave nondestructive testing and evaluation[1]. Such a characterization can be realized by non-resonance based methods thanks to their broadband nature, relatively relaxed sample preparation requirement, and widespread implementability over many distinct application areas involving composition analysis and cure state monitoring of cement-based structures, detection of conductive filler in rubber composites, and examining porosity level in ceramics[2,3]. Among many non-resonance based methods (planar, coaxial, waveguide, free-space, etc.), free-space non-resonance based methods have distinct advantages involving simplicity of analysis in frequency-domain[4–22] or time-domain[23–27] and non-contact measurements, especially for measurements at harsh environmental conditions[6].

There are four main scenarios considered in the analysis of free-space methods: i) implementation using reflection-only[15,18], transmission-only[12,17], or reflection and transmission measurements[8,13], ii) dependence on partially-calibrated or self-calibrated (without determining elements of any error networks) measurements[12,14,16,18], iii) extraction relying on analytical expressions without utilizing any numerical tool or vice versa[8,11], and iv) electromagnetic parameter retrieval of thin materials[19]. It is noted that while reflection-only free-space measurements provide sufficient information for material characterization and are suitable for measurements of samples whose rear side is not achievable[17,20,22], reflection and transmission free-space measurements give additional information for the same goal[19] and are feasible for through-wall applications[28]. Free-space methods requiring sample thickness information are highly dependent on sample thickness information for an accurate electromagnetic parameter determination[21], especially for thinner samples due to fabrication tolerances. In addition, free-space methods based on any formal calibration procedure[4–13,15,17,19,22] are limited by a proper calibration procedure based on calibration standards. To eliminate such a dependence, self-calibrated or partial-calibrated free-space methods relying on self-calibration procedures[14,16,18–21] can be exercised. Besides, free-space methods utilizing a numerical toolbox suffer from improper initial guess for electromagnetic properties of the sample. Finally, electromagnetic property measurement of thin materials is also important due to its importance in many diverse fields including microwave absorbers[29]. In the present study, our goal is to propose a free-space electromagnetic extraction procedure for electrically thin samples relying on an improved self-calibrated procedure using reflection and transmission measurements without resorting to any numerical toolbox.

ARTICLE IN PRESS

Table 1. Comparison of some free-space reflection/transmission extraction methods

Study	Measurement Type	Error Network for Antennas	Reflection Property of Error Networks	Reciprocal or Non-reciprocal
[14]	Reflection	One Two-Port Network	Negligible or Zero-Reflection	Reciprocal
[18]	Reflection	One Two-Port Network	Negligible or Zero-Reflection	Nonreciprocal
[20]	Reflection	One Two-Port Network	Negligible or Zero-Reflection	Reciprocal
[16]	Reflection/Transmission	Identical Two Two-Port Networks	Zero-Reflection	Reciprocal
[19]	Reflection/Transmission	Non-Identical Two Two-Port Networks	Zero-Reflection	Reciprocal
[21]	Reflection/Transmission	Identical Two Two-Port Networks	Non-Zero Reflection	Reciprocal
Proposed	Reflection/Transmission	Non-Identical Two Two-Port Networks	Non-Zero Reflection	Nonreciprocal

When the free-space methods[14,16,18–21] using self-calibrated or partial-calibrated are examined, it is noted that only those in the studies[16,19,21] utilize both reflection and transmission free-space measurements, which are our concern in this study. The free-space extraction methods[16,19,21] use two two-port networks to take into account of transmitting and receiving antenna regions. These models in the studies[16,21] assume identical two two-port networks. However, such an assumption is hard to fully realize in real applications due to some fabrication tolerances that may appear even if transmitting and receiving antennas are fabricated from the same batch. The error network model in the study[19] can be utilized to relax this stringent requirement. Nonetheless, this method considers that these networks have zero internal reflection. Such a consideration can result in reduced accuracy for antennas having large internal reflections, which then produce ripples in the extracted ε_r due to ringing between the sample and antenna. Table 1 presents a brief comparison of our proposed method with other reflection-only free-space methods[14,18,20] and reflection-transmission free-space methods[16,19,21] using calibration error networks in the extraction procedure in terms of measurement type, properties of error networks, whether error networks involve zero or non-zero reflection, and whether error networks are reciprocal or non-reciprocal.

In this paper, dissimilar from the studies[16,19,21], transmitting and receiving antenna region error networks are considered to be non-reciprocal and non-identical with zero or non-zero reflection asymmetric feature to improve ε_r determination. A metric function with no dependence on the terms of the transmitting and receiving antenna networks and with no reference plane transformation information is determined for accurate and stable ε_r extraction. The remaining part of our paper is formatted as follows. First, the proposed method along with derived objective functions for ε_r determination is presented in Section 2. Next, results of a numerical analysis for validation of our method are analyzed in Section 3. Then, analysis of angle misalignment effect is followed in Section 4. After, discussion of measurement results of two low-loss and electrically thin samples is given in Section 5, and pros and cons of our method are mentioned in Section 6. Finally, all relevant points are recapitulated in Section 7.

ARTICLE IN PRESS

2 The Proposed Method

2.1 Description of Error Matrices and Sample Region

Fig. 1 illustrates a schematic description of a free-space measurement environment involving five distinct regions, three of which are described by full two-port networks (transmitting and receiving antenna regions in addition to the sample region) and two of which are described by simplified two-port networks (reflection-free air regions). While $S_{11}^{(a)}$ and $S_{21}^{(a)}$ are the forward scattering (S-) parameters and $S_{12}^{(a)}$ and $S_{22}^{(a)}$) are the backward S-parameters of the transmitting antenna region $[T]$, $S_{11}^{(b)}$ and $S_{21}^{(b)}$ are the forward S-parameters and $S_{12}^{(b)}$ and $S_{22}^{(b)}$ are the backward S-parameters of the receiving antenna region $[R]$. In a similar fashion, S_{11}, S_{21}, S_{12}, and S_{22} are the forward and backward reflection and transmission S-parameters of the sample $[S]$. On the other hand, R_{01} and R_{02} are the (forward or backward) transmission S-parameters of the air regions $[A1]$ and $[A2]$, respectively. It is noted that the free-space model considered here is more general than that considered in the study[16], which assumes $S_{11}^{(a)} = S_{22}^{(a)} = S_{11}^{(b)} = S_{22}^{(b)} = 0$ and $S_{21}^{(a)} = S_{12}^{(a)} = S_{21}^{(b)} = S_{12}^{(b)}$ and that examined in the study[19], which uses $S_{11}^{(a)} = S_{22}^{(a)} = S_{11}^{(b)} = S_{22}^{(b)} = 0$, $S_{21}^{(a)} = S_{12}^{(a)} = T_a$, and $S_{21}^{(b)} = S_{12}^{(b)} = T_b$, and that formulated in the study[21], which utilizes $S_{11}^{(a)} = S_{22}^{(b)}$, $S_{11}^{(b)} = S_{22}^{(a)}$, $S_{12}^{(a)} = S_{21}^{(a)}$, and $S_{12}^{(b)} = S_{21}^{(b)}$.

For the cascaded network description in Fig. 1, it is possible to apply wave-cascading matrices, transfer matrices, or state-transition matrices to examine overall reflection and transmission properties of the entire system. However, we will prefer using S-parameter description of this cascaded network description, although partly complicates the analysis, because determinant of a two-port S-parameter description is free from the effects of rotations (reference-plane-invariant property)[30]. The overall system in Fig. 1 can be evaluated using the sub-models in Figs. 2(a) and 2(b) for forward reflection and transmission S-parameters, respectively. In these sub-models, Γ_f^{sam} and Γ_b^{sam} refer to the equivalent reflection S-parameters seen at the forward and backward directions whereas T_f^{sam} presents the equivalent transmission S-parameter seen at the forward direction[31].

Utilizing the sub-models in Figs. 2(a) and 2(b), one can determine the forward reflection and transmission S-parameters of

ARTICLE IN PRESS

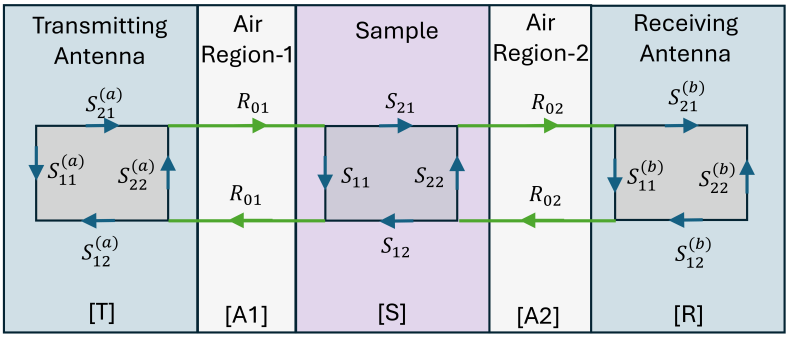

Figure 1. A schematic description of a free-space measurement environment involving three full two-port networks (transmitting antenna region $[T]$, receiving antenna region $[R]$, and the sample region $[S]$) and two simplified two-port networks (reflection-free air regions $[A1]$, and $[A2]$).

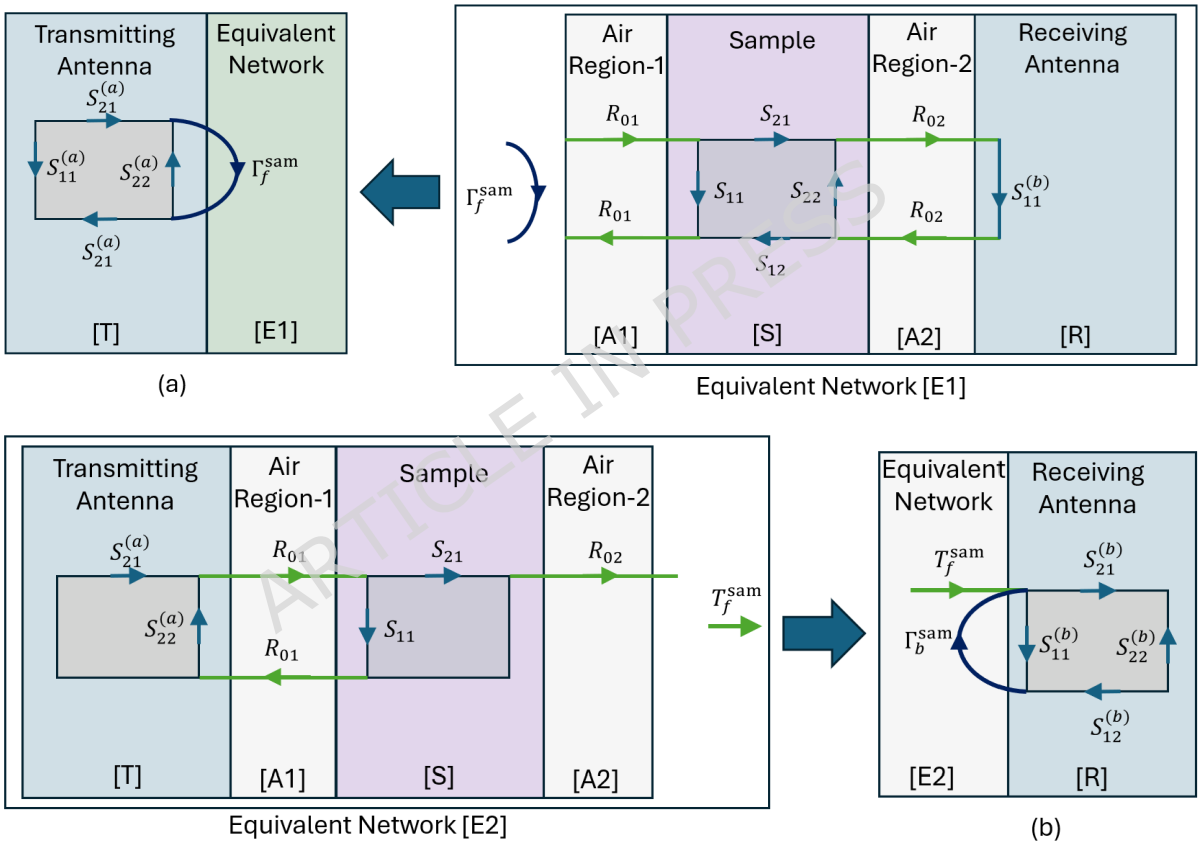

Figure 2. Sub-models for the analysis of forward (a) reflection and (b) transmission S-parameters of the measurement system. Here, Γ_f^{sam} and Γ_b^{sam} are the equivalent reflection S-parameters while T_f^{sam} is the equivalent transmission S-parameter.

the entire system (S_{11}^{sam} and S_{21}^{sam}) as

$$S_{11}^{sam} = S_{11}^{(a)} + \frac{S_{21}^{(a)} S_{12}^{(a)} \Gamma_f^{sam}}{1 - \Gamma_f^{sam} S_{22}^{(a)}}, \tag{1}$$

$$S_{21}^{sam} = \frac{S_{21}^{(b)} T_f^{sam}}{1 - \Gamma_b^{sam} S_{11}^{(b)}}, \tag{2}$$

ARTICLE IN PRESS

where

$$\Gamma_f^{\text{sam}} = R_{01}^2 \left(S_{11} + \frac{R_{02}^2 S_{21} S_{12} S_{11}^{(\text{b})}}{1 - R_{02}^2 S_{22} S_{11}^{(\text{b})}} \right), \tag{3}$$

$$\Gamma_b^{\text{sam}} = R_{02}^2 \left(S_{22} + \frac{R_{01}^2 S_{12} S_{21} S_{22}^{(\text{a})}}{1 - R_{01}^2 S_{11} S_{22}^{(\text{a})}} \right), \tag{4}$$

$$T_f^{\text{sam}} = R_{01} R_{02} \frac{S_{21} S_{21}^{(\text{a})}}{1 - R_{01}^2 S_{11} S_{22}^{(\text{a})}}. \tag{5}$$

Following a similar procedure, the backward reflection and transmission S-parameters of the entire system (S_{22}^{sam} and S_{12}^{sam}, respectively) can be obtained as

$$S_{22}^{\text{sam}} = S_{22}^{(\text{b})} + \frac{S_{12}^{(\text{b})} S_{21}^{(\text{b})} \Gamma_b^{\text{sam}}}{1 - \Gamma_b^{\text{sam}} S_{11}^{(\text{b})}}, \tag{6}$$

$$S_{12}^{\text{sam}} = \frac{S_{12}^{(\text{a})} T_b^{\text{sam}}}{1 - \Gamma_f^{\text{sam}} S_{22}^{(\text{a})}}, \tag{7}$$

where

$$T_b^{\text{sam}} = R_{01} R_{02} \frac{S_{12} S_{12}^{(\text{b})}}{1 - R_{02}^2 S_{22} S_{11}^{(\text{b})}}. \tag{8}$$

It is noted that symmetry exits between forward and backward reflection (and transmission) S-parameters in (1)-(8). For example, S_{12}^{sam} can be evaluated from (2) by proper interchange of parameters.

For the case after the sample is removed from the arrangement in Fig. 1 (air-filled region), forward and backward S-parameters of this arrangement (S_{11}^{air}, S_{21}^{air}, S_{12}^{air}, and S_{22}^{air}) will have the following expressions

$$S_{11}^{\text{air}} = S_{11}^{(\text{a})} + \frac{S_{21}^{(\text{a})} S_{12}^{(\text{a})} \Gamma_f^{\text{air}}}{1 - \Gamma_f^{\text{air}} S_{22}^{(\text{a})}}, \tag{9}$$

$$S_{21}^{\text{air}} = \frac{S_{21}^{(\text{b})} T_f^{\text{air}}}{1 - \Gamma_b^{\text{air}} S_{11}^{(\text{b})}}, \tag{10}$$

$$S_{22}^{\text{air}} = S_{22}^{(\text{b})} + \frac{S_{12}^{(\text{b})} S_{21}^{(\text{b})} \Gamma_b^{\text{air}}}{1 - \Gamma_b^{\text{air}} S_{11}^{(\text{b})}}, \tag{11}$$

$$S_{12}^{\text{air}} = \frac{S_{12}^{(\text{a})} T_b^{\text{air}}}{1 - \Gamma_f^{\text{air}} S_{22}^{(\text{a})}}, \tag{12}$$

where

$$\Gamma_f^{\text{air}} = R_{01}^2 R_{02}^2 S_{21}^0 S_{12}^0 S_{11}^{(\text{b})}, \tag{13}$$

$$\Gamma_b^{\text{air}} = R_{02}^2 R_{01}^2 S_{12}^0 S_{21}^0 S_{22}^{(\text{a})}, \tag{14}$$

$$T_f^{\text{air}} = R_{01} R_{02} S_{21}^0 S_{21}^{(\text{a})}, \tag{15}$$

$$T_b^{\text{air}} = R_{01} R_{02} S_{12}^0 S_{12}^{(\text{b})}. \tag{16}$$

It is noteworthy that $S_{11} = S_{22} = 0$, $S_{21} \to S_{21}^0$, and $S_{12} \to S_{12}^0$ for this new arrangement.

ARTICLE IN PRESS

2.2 Determination of Relative Complex Permittivity Free From Error Networks and Reference Plane Transformation Factors

Given the expressions of S_{11}^{sam}, S_{21}^{sam}, S_{12}^{sam}, and S_{22}^{sam} in (1), (2), (6), and (7) and the expressions of S_{11}^{air}, S_{21}^{air}, S_{12}^{air}, and S_{22}^{air} in (9)-(12), the determinant of S-parameters corresponding to the sample and air cases can be obtained as

$$S_{11}^{\text{u}}S_{22}^{\text{u}} - S_{21}^{\text{u}}S_{12}^{\text{u}} = \Delta S_{\text{u}} = \frac{S_{11}^{(\text{a})}S_{22}^{(\text{b})} - S_{21}^{(b)}S_{12}^{(a)}T_f^{\text{u}}T_b^{\text{u}} - \Delta S_a S_{22}^{(\text{b})}\Gamma_f^{\text{u}} + \Delta S_b\Gamma_b^{\text{u}}\left(\Delta S_a\Gamma_f^{\text{u}} - S_{11}^{(\text{a})}\right)}{\left[1-\Gamma_b^{\text{u}}S_{11}^{(\text{b})}\right]\left[1-\Gamma_f^{\text{u}}S_{22}^{(\text{a})}\right]}, \tag{17}$$

where u = 'sam' or 'air' and

$$\Delta S_a = S_{11}^{(\text{a})}S_{22}^{(\text{a})} - S_{12}^{(\text{a})}S_{21}^{(\text{a})}, \qquad \Delta S_b = S_{11}^{(\text{b})}S_{22}^{(\text{b})} - S_{12}^{(\text{b})}S_{21}^{(\text{b})}. \tag{18}$$

Similarly, hybrid products of reflection S-parameters of the sample and air regions yield

$$\begin{aligned} S_{11}^{\text{sam}}S_{22}^{\text{air}} - S_{11}^{\text{air}}S_{22}^{\text{sam}} &= S_{\text{mix}} \\ &= \left[\frac{S_{11}^{(\text{a})} - \Delta S_a\Gamma_f^{\text{sam}}}{1-\Gamma_f^{\text{sam}}S_{22}^{(\text{a})}}\right]\left[\frac{S_{22}^{(\text{b})} - \Delta S_b\Gamma_b^{\text{air}}}{1-\Gamma_b^{\text{air}}S_{11}^{(\text{b})}}\right] \\ &+ \left[\frac{S_{11}^{(\text{a})} - \Delta S_a\Gamma_f^{\text{air}}}{1-\Gamma_f^{\text{air}}S_{22}^{(\text{a})}}\right]\left[\frac{S_{22}^{(\text{b})} - \Delta S_b\Gamma_b^{\text{sam}}}{1-\Gamma_b^{\text{sam}}S_{11}^{(\text{b})}}\right]. \end{aligned} \tag{19}$$

It is clearly seen from (17)-(19) that ΔS_{sam}, ΔS_{air}, and S_{mix} vary with ΔS_a and ΔS_b. If the sample has reflection symmetric property and is reciprocal, one can evaluate[21]

$$S_{11} = S_{22} = \frac{\Gamma(1-T^2)}{1-\Gamma^2T^2}, \quad S_{21} = S_{12} = \frac{T(1-\Gamma^2)}{1-\Gamma^2T^2}, \tag{20}$$

$$\Gamma = \frac{1-\sqrt{\varepsilon_r}}{1+\sqrt{\varepsilon_r}}, \quad T = e^{-jk_0\sqrt{\varepsilon_r}W}, \quad \varepsilon_r = \varepsilon_r' - j\varepsilon_r'', \tag{21}$$

where the surface reflection coefficient and propagation factor in the sample are denoted by Γ and T, respectively, and the sample thickness and free-space wavenumber are represented by W and k_0, respectively.

On the other hand, the transmission S-parameters for the air region [A1] with length L_{01}, the air region [A2] with length L_{02}, and the air region with length W (no sample is present) in Fig. 1 can be evaluated from

$$R_{01} = e^{-jk_0L_{01}}, \quad R_{02} = e^{-jk_0L_{02}}, \quad T_0 = e^{-jk_0W}. \tag{22}$$

It is obvious from (17) and (19) that ΔS_{sam}, ΔS_{air}, and S_{mix} are not only all functions of error network terms ($S_{11}^{(\text{a})}$, $S_{21}^{(\text{a})}$, $S_{212}^{(\text{a})}$, $S_{22}^{(\text{a})}$) and but also are dependent on reference plane transformation factors R_{01} and R_{02}. Similar to the study[21], the following objective function can be ascertained after utilizing ΔS_{sam}, ΔS_{air}, and S_{mix} in (17)-(19)

$$\begin{aligned} F_{\text{obj}} &= \frac{S_{\text{mix}} - \Delta S_{\text{sam}} - \Delta S_{\text{air}}}{S_{21}^{\text{sam}}S_{21}^{\text{air}}} = \frac{T_0^2(1-\Gamma^2T^2) + (T^2 - T_0^2)}{T_0T(1-\Gamma^2)} \\ &= \left[1 + \frac{1}{2}\left(\sqrt{\varepsilon_r} + \frac{1}{\sqrt{\varepsilon_r}}\right)\right]\cos\left[(1-\sqrt{\varepsilon_r})k_0W\right] \\ &+ \left[1 - \frac{1}{2}\left(\sqrt{\varepsilon_r} + \frac{1}{\sqrt{\varepsilon_r}}\right)\right]\cos\left[(1+\sqrt{\varepsilon_r})k_0W\right] \end{aligned} \tag{23}$$

It is clear from the expression of F_{obj} in (23) that ε_r can be directly evaluated from measured S-parameters without resorting to the information of the error network terms and reference plane transformation factors. Such an evaluation, however, requires a 2D numerical methodology such as the Newton-Raphson method. There are two drawbacks of such a computation. First, numerical methods necessitate a good initial guess to converge to a global minimum. Second, 2D numerical methods require more computational time than 1D numerical methods necessitate (e.g., internal halving or bisection method)[32]. After

ARTICLE IN PRESS

ARTICLE IN PRESS

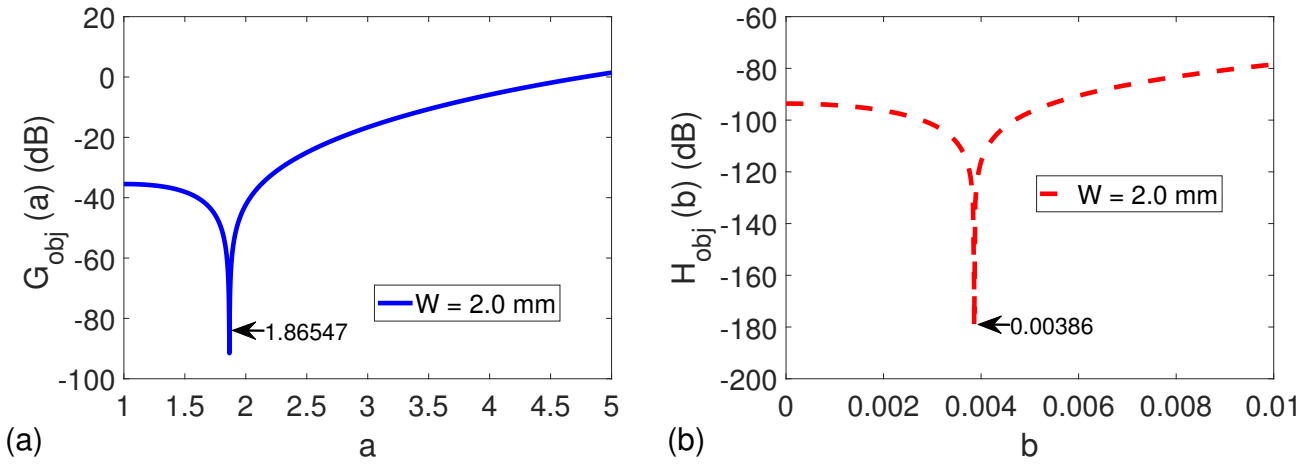

Figure 3. Dependencies of (a) $G_{\text{obj}}(a)$ versus a and (b) $H_{\text{obj}}(b)$ versus b of the tested sample ($W = 2.00$ mm).

considering these points, letting $\sqrt{\varepsilon_r} = a - jb$ and $\phi_0 = k_0 W$, and assuming $\sinh(b\phi_0) \approx b\phi_0$ and $\cosh(b\phi_0) \approx 1.0$ for electrically thinner samples ($W < \lambda/4$ where λ is the sample wavelength), the following useful objective function is derived to evaluate a only

$$G_{\text{obj}}(a) \approx 0 = \left| F_{\text{obj}}^{\text{real}} - \left(a + \frac{1}{a}\right) \sin(a\phi_0)\sin(\phi_0) + 2\cos(a\phi_0)\cos(\phi_0) \right|, \tag{24}$$

where $F_{\text{obj}}^{\text{real}}$ is the real part of F_{obj}, and $|\star|$ denotes the magnitude of '$\star$'. Even though the objective function given in (24) is identical to that in the study[21], our model in Fig. 1 is more general than that was considered in the study[21]. For example, the new model examined in Fig. 1 considers that there is no need that the transmitting and receiving antennas are identical having the same reflection and transmission properties $S_{11}^{(a)} = S_{22}^{(b)}$, $S_{22}^{(a)} = S_{11}^{(b)}$, $S_{21}^{(b)} = S_{12}^{(b)}$, and $S_{12}^{(a)} = S_{21}^{(b)}$.

After substituting the calculated a from (24), b can be computed by a suitable 1D numerical method from

$$\begin{aligned} H_{\text{obj}}(b) \approx 0 = & \left| F_{\text{obj}}^{\text{real}} - \left[\left(\frac{b}{a^2+b^2} - b \right) \cos(a\phi_0)\sinh(b\phi_0) \right.\right. \\ & \left.\left. + \left(\frac{a}{a^2+b^2} + a \right) \sin(a\phi_0)\cosh(b\phi_0) \right] \sin(\phi_0) \right. \\ & \left. + 2\cos(\alpha\phi_0)\cos(\phi_0)\cosh(b\phi_0) \right|. \end{aligned} \tag{25}$$

Finally, ε_r can be determined from

$$\varepsilon_r' = a^2 - b^2, \quad \varepsilon_r'' = 2ab. \tag{26}$$

It is noted that the derived objective functions in (24) and (25) are applicable for electrically thin low-loss samples, which are our main concern in the present study.

3 Validation

In this section, a numerical analysis is considered to validate the derived objection functions $G_{\text{obj}}(a)$ in (24) and $H_{\text{obj}}(b)$ in (25). Toward this end, the parameters, selected arbitrarily just for the demonstration purpose, were considered: $S_{11}^{(a)} = 0.1 - j0.4$, $S_{21}^{(a)} = S_{12}^{(a)} = 0.5 + j0.4$, $S_{22}^{(a)} = -0.2 - j0.2$, $S_{11}^{(b)} = 0.1 + j0.2$, $S_{21}^{(b)} = S_{12}^{(b)} = -0.2 + j0.4$, and $S_{22}^{(b)} = -0.7 - j0.1$, $L_{01} = 40$ cm,

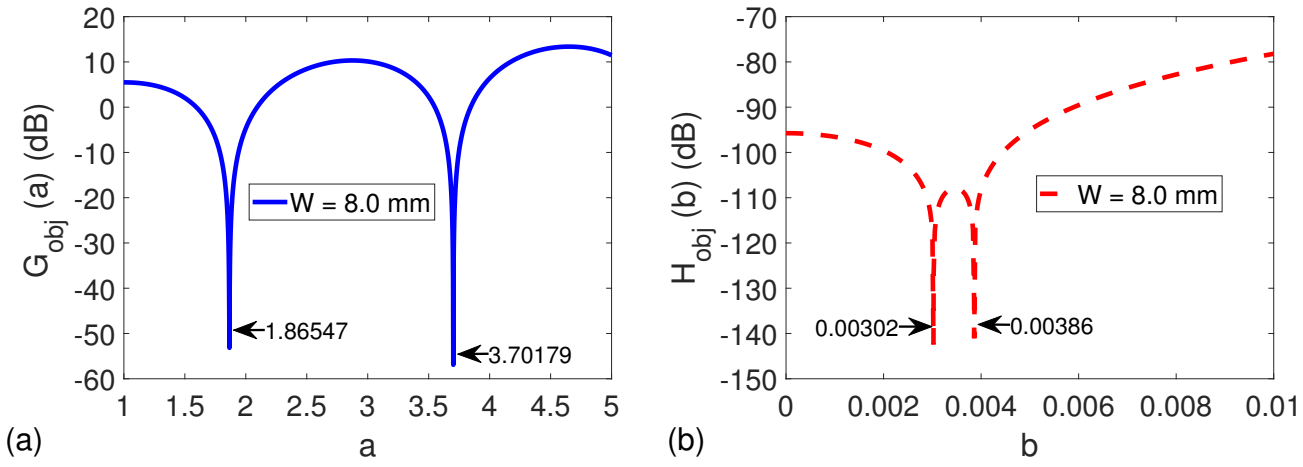

Figure 4. Dependencies of (a) $G_{\text{obj}}(a)$ versus a and (b) $H_{\text{obj}}(b)$ versus b of the tested sample when $W = 8.00$ mm.

and $L_{02} = 42$ cm ($L_{01} = L_{02}$ could also be used). In addition, it was assumed that the sample had $\varepsilon_r = 3.48(1 - j0.0037)$ (Rogers 4350B)[21,33], $W = 2.0$ mm, and $f = 10.3$ GHz (mid-frequency) after taking into account of the measurement configuration given in Section 5. For this selection, it is noted that $\lambda \approx 15.6$ mm and $W \ll \lambda/4$. Figs. 3(a) and 3(b) demonstrate, respectively, the dependencies of $G_{\text{obj}}(a)$ versus a and $H_{\text{obj}}(b)$ versus b for the tested sample. It is seen from Figs. 3(a) and 3(b) that there is only one a value and one b value, which are very close to the actual values of ≈ 1.86547 and ≈ 0.00386 [$\varepsilon_r \cong 3.479(1 - j0.0040)$] ($\Delta\varepsilon_r' \leq 1\%$ and $\Delta\varepsilon_r'' \leq 8\%$), validating the derived $G_{\text{obj}}(a)$ in (24) and $H_{\text{obj}}(b)$ in (25). To evaluate the effect of increased sample length on a computation using $G_{\text{obj}}(a)$ in (24) and $H_{\text{obj}}(b)$ in (25), they were re-drawn as shown in Figs. 4(a) and 4(b) for the tested sample with $W = 8.0$ mm (all the remaining parameters are the same). It is seen from the results in Figs. 4(a) and 4(b) that there are more than one a and b pair producing minimum $G_{\text{obj}}(a)$ and $H_{\text{obj}}(b)$ when $W > \lambda/4$, meaning that $G_{\text{obj}}(a)$ in (24) and $H_{\text{obj}}(b)$ in (25) are effective for electrically thinner samples ($W < \lambda/4$) only for unique ε_r determination. As a consequence, the maximum thickness $W_{\max}$ that $G_{\text{obj}}(a)$ is applicable is limited by $W_{\max} \leq \lambda/4$ or $W_{\max} \leq \lambda_0/(4a)$ where λ_0 is the free-space wavelength.

4 Effect of Sample Misalignment

In our previous study[21], sensitivity and uncertainty analyses were performed utilizing closed-form expressions and GUM-based uncertainty model[34]. Such analyses are important to evaluate the performance of a new extraction method. Although our new model in Fig. 1 is more general than that in Fig. 1 of our previous study[21], as noted in Sections 1 and 5, the fundamental objective functions ((23) in our present study and (18) in the study[21]) are identical. Therefore, sensitivity and uncertainty analyses performed in the study[21] are still applicable for our new model in Fig. 1. However, not mentioned and examined in that study[21] was the effect of sample misalignment on ε_r evaluation. To fill in this gap, in the present study, sample misalignment effect was examined.

To achieve our goal, 3D simulations using CST Microwave Studio were carried out. To realize a sample with a theoretically infinite transverse plane, unit cell boundary conditions were implemented over the transverse plane of the sample in the frequency domain by selecting the tetrahedral mesh-type (adaptive meshing) to perform the simulations precisely. Simulations were conducted at X-band (8.2 - 12.4 GHz) with 1001 frequency (default) points. Figs. 5(a) and 5(b) illustrate, respectively, the dependencies of $G_{\text{obj}}(a)$ versus a and $H_{\text{obj}}(b)$ versus b for the tested sample ($W = 2.00$ mm) under different incidence angle (θ_{in}) values. It is seen from Figs. 5(a) and 5(b) that our proposed method requires precise positioning for an accurate a and b determination, since $G_{\text{obj}}(a)$ and $H_{\text{obj}}(b)$ are chiefly sensitive to θ_{in}. Besides, Figs. 6(a) and 6(b) demonstrate, respectively, the percentage variations ($\Delta\varepsilon_r'$ and $\Delta\varepsilon_r''$) of ε_r' and ε_r'' versus incidence angles. It is noted from the results in Figs. 6(a) and 6(b) that precise sample positioning is critical for an accurate ε_r determination (especially for ε_r'' because the sample is a very low-loss sample).

5 Measurement Results and Discussion

Fig. 7 presents a photo of the free-space measurement setup used to validate our proposed method. This setup includes a vector network analyzer (VNA), manufactured by the Keysight Technologies (Model: N9918A), to perform 2-port S-parameter

ARTICLE IN PRESS

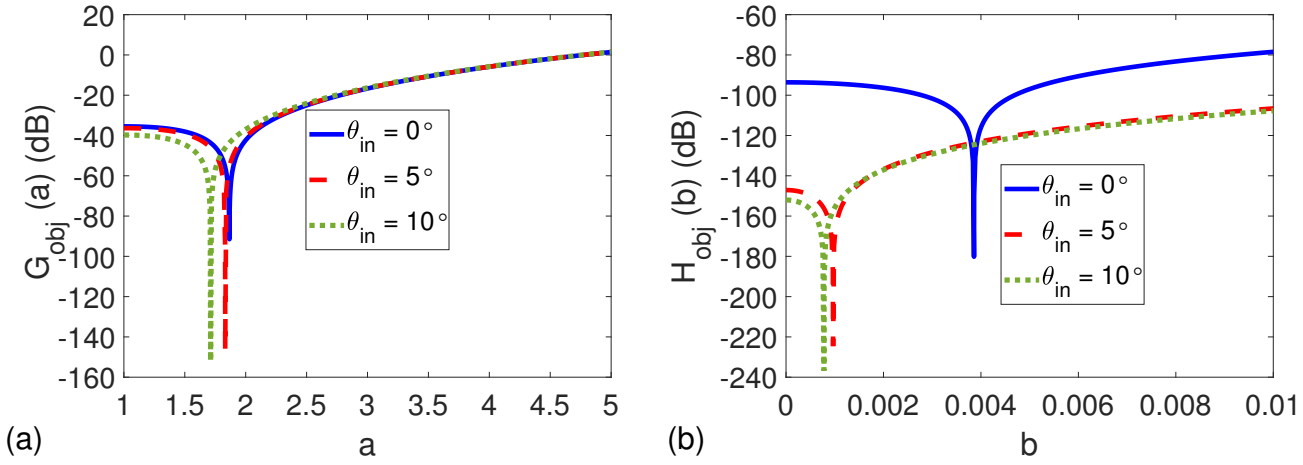

Figure 5. Dependencies of (a) $G_{\mathrm{obj}}(a)$ versus a and (b) $H_{\mathrm{obj}}(b)$ versus b of the tested sample ($W = 2.00$ mm) under different incidence angle (θ_{in}) values.

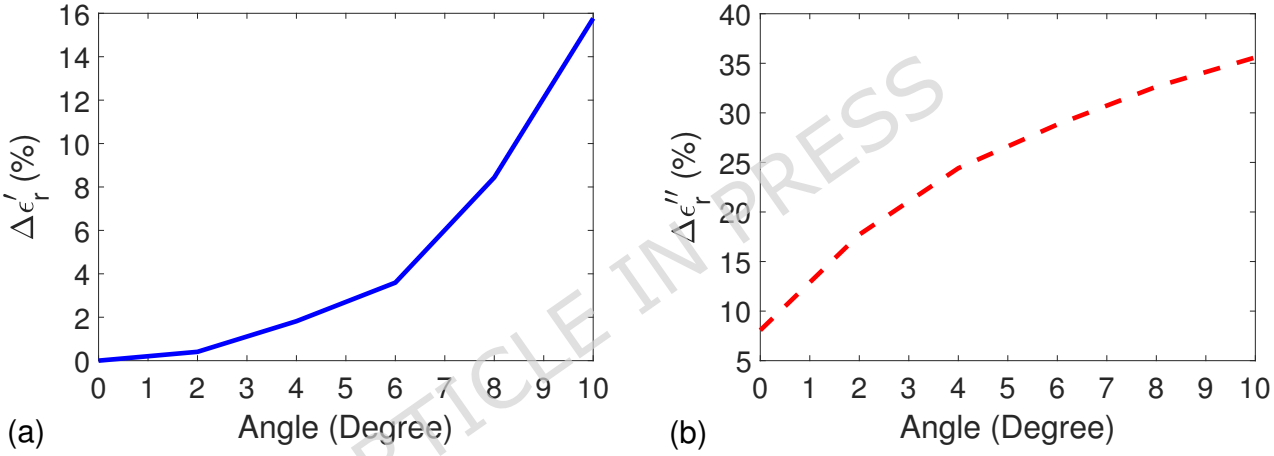

Figure 6. Percentage variations of (a) ε_r' and (b) ε_r'' versus incidence angles of the tested sample ($W = 2.00$ mm).

measurements at X-band. Electromagnetic signals generated by the VNA are carried out by two coaxial lines to identical horn-lens antennas, manufactured by the Flann Microwave Instruments (Series 820). Our theoretical model assumes that the sample is positioned at the far-field (or far-zone) of the transmitting and receiving antennas. For an ordinary lens-free (lensless) antenna, the far-field location could be set to a distance at least the limit of $2D^2/\lambda$ where D is the largest dimension of the antenna (the diagonal distance for rectangular antennas and diameter for circular antennas) and λ is the wavelength. As seen from this expression, this criterion can be safely met by considering the minimum frequency of the operating frequency band. Besides, free-space measurements can suffer from diffraction effects arising from sharp edges or corners of a sample and (spherical) wave spreading effects while wave is propagating. These two effects set a limit for the transverse dimensions of the analyzed sample. A a rule of thumb, transverse dimensions (sizes) of the sample should be selected to be greater than at least 3 times the footprint (or -10 dB beam diameter) of the quasi-Gaussian beam at the sample surface[6]. Since achieving the far-field approximation and suppressing the aforementioned effects in a free-space setup are partly difficult for a lens-free antenna, in our measurement, we utilized a horn-lens antenna for convenience. Then, samples were positioned approximately 40 cm away from both transmitting and receiving antennas to implement far-field criterion, after following the antenna manual and performing some preliminary measurements. Besides, it is observed that samples with at least transverse dimensions of 20cm×20cm has sufficient accuracy[21] to mitigate, if not totally eliminate, diffraction and wave spreading effects in our measurement setup.

Different from our previous study in[21], here two different measurement scenarios were considered in our present study. The first scenario (NZR-1 case) assumes that the two coaxial lines are identical with a length of 100 cm. The second scenario

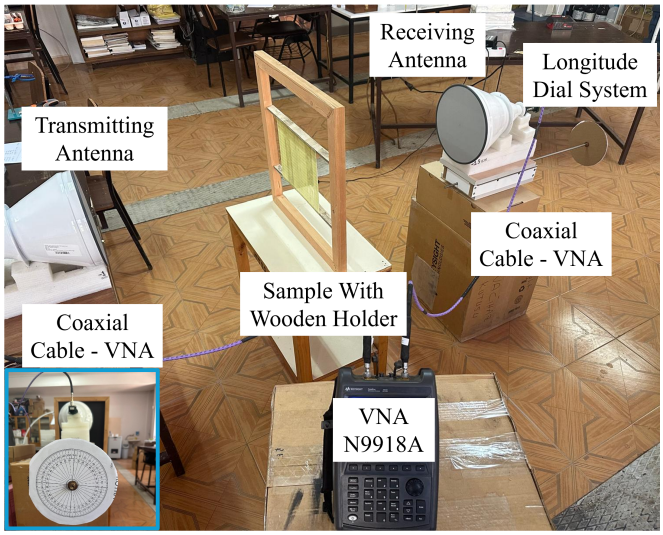

Figure 7. Measurement setup for validation of our proposed method.

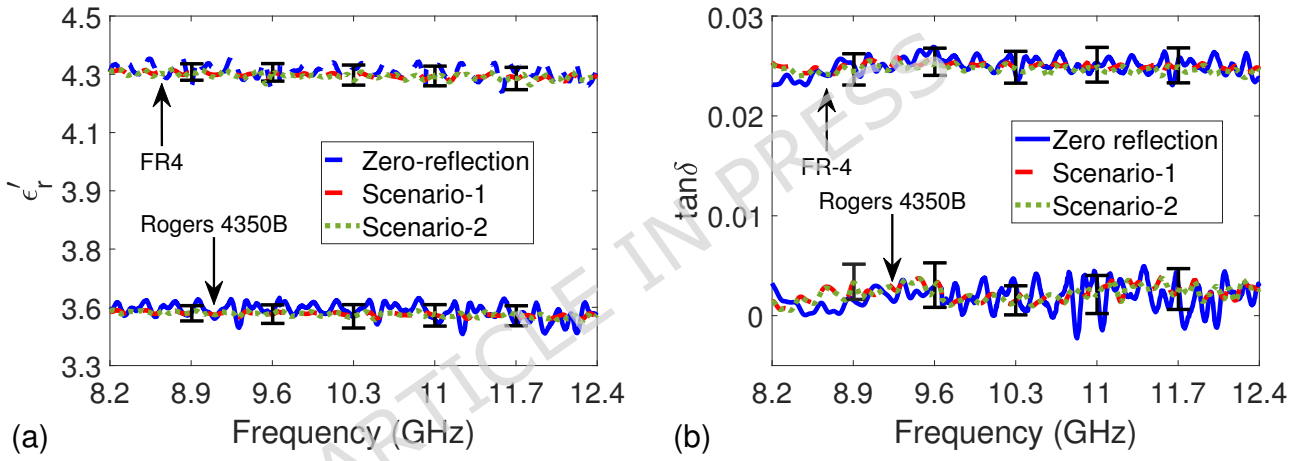

Figure 8. Measured (a) ε_r' and (b) tanδ of the tested Rogers 4350B and FR-4 samples by the proposed method for difference cases: i) Zero reflection ($S_{11}^{(a)} = 0$ and $S_{22}^{(a)} = 0$), ii) Scenario-1 involving $S_{11}^{(a)} \neq 0$ and $S_{22}^{(a)} \neq 0$ (two identical coaxial lines), and iii) Scenario-2 involving $S_{11}^{(a)} \neq 0$ and $S_{22}^{(a)} \neq 0$ (two non-identical coaxial lines).

(NZR-2 case) considers that the first coaxial line is the same as the previous case, but the length of the second coaxial line is doubled (two identical coaxial lines each of which has a length of 100 cm are cascaded sequentially). This means that while the first scenario is the scenario that was considered in our previous study[21], the second scenario is a new one, which exemplifies the free-space model given in Fig. 1. Two different samples[21] with diverse ε_r' and ε_r'' values were tested to assess the performance of the proposed method. These samples are the Rogers 4350B sample ($W \approx 1.52$ mm) and the FR4 sample ($W \approx 1.60$ mm) with their lengths measured by a high precision caliper with a resolution of 0.05 mm over 200 mm scale (from Mitutoyo with a dial reading).

A rectangular hollow wooden frame (around 40×40 cm^2) was utilized to firmly hold the samples to eliminate angle misalignment inline with the results in Section 4. Tested samples were sequentially positioned around the center of the frame. A longitudinal stage was used to precisely arrange the distance between either antenna and the sample surface (see the inset of Fig. 7). S-parameter measurements (total of 1001 frequency points linearly located at X-band) were iterated five times for each sample to examine repeatability of the extraction methods to be discussed shortly.

Figs. 8(a) and 8(b) show, respectively, the extracted ε_r' and ε_r'' of the tested Rogers 4350B and FR-4 samples under three different cases using averaged S-parameters of five independent measurements along with the rolling average method

ARTICLE IN PRESS

Table 2. Evaluated ε_r and tanδ of the Rogers 4350B sample at some discrete frequencies ($f = 8.2$ GHz, 10.3 GHz, and 12.4 GHz) for three different cases: i) ZR case[16,19], ii) NZR-1 case[21], and iii) NZR-2 (the model in Fig. 1 in the present study)

	Case	$f = 8.2$ GHz	$f = 10.3$ GHz	$f = 12.4$ GHz
ε_r'	ZR	$3.49 \mp 4.12\%$	$3.47 \mp 4.35\%$	$3.47 \mp 4.78\%$
	NZR-1	$3.48 \mp 3.47\%$	$3.47 \mp 3.12\%$	$3.47 \mp 3.45\%$
	NZR-2	$3.48 \mp 3.43\%$	$3.47 \mp 3.10\%$	$3.47 \mp 3.46\%$
tanδ	ZR	$0.0032 \mp 8.11\%$	$0.0030 \mp 8.78\%$	$0.0029 \mp 9.67\%$
	NZR-1	$0.0014 \mp 6.12\%$	$0.0015 \mp 5.89\%$	$0.0027 \mp 6.26\%$
	NZR-2	$0.0013 \mp 5.97\%$	$0.0015 \mp 5.56\%$	$0.0026 \mp 6.25\%$

Table 3. Evaluated ε_r and tanδ of the FR-4 sample at some discrete frequencies ($f = 8.2$ GHz, 10.3 GHz, and 12.4 GHz) for three different cases: i) ZR case[16,19], ii) NZR-1 case[21], and iii) NZR-2 (the model in Fig. 1 in the present study)

	Case	$f = 8.2$ GHz	$f = 10.3$ GHz	$f = 12.4$ GHz
ε_r'	ZR	$4.31 \mp 3.63\%$	$4.32 \mp 3.48\%$	$4.31 \mp 4.01\%$
	NZR-1	$4.31 \mp 2.84\%$	$4.30 \mp 2.75\%$	$4.29 \mp 2.64\%$
	NZR-2	$4.31 \mp 2.83\%$	$4.30 \mp 2.75\%$	$4.29 \mp 2.64\%$
tanδ	ZR	$0.023 \mp 8.35\%$	$0.024 \mp 8.41\%$	$0.023 \mp 8.95\%$
	NZR-1	$0.025 \mp 6.38\%$	$0.024 \mp 6.11\%$	$0.023 \mp 5.98\%$
	NZR-2	$0.025 \mp 6.35\%$	$0.024 \mp 6.13\%$	$0.023 \mp 5.78\%$

implemented for ten frequency points to eliminate residual parasitic signals[21]. These figures also indicate the percentage variations of ε_r and tanδ at frequencies 8.9 GHz, 9.6 GHz, 10.3 GHz, 11.0 GHz, and 11.7 GHz for the proposed method. The first case (ZR case) assumes that the transmitting and reflecting antennas have the same matrices ($[T] = [R]$) with no internal reflections ($S_{11}^{(a)} = 0$ and $S_{22}^{(a)} = 0$). This case was taken into account in the studies[14,16,18] and in the studies[19,20] (with no time-gating procedure). The second case (NZR-1) exemplifies that the transmitting and reflecting antennas have the same matrices ($[T] = [R]$) with non-identical and non-zero reflections ($S_{11}^{(a)} \neq S_{22}^{(a)} \neq 0$), which has been considered in our recent study[21]. The final case (NZR-2), which is analyzed in the present study, models the most general case that the transmitting and reflecting antennas have different matrices ($[T] \neq [R]$) involving non-identical and non-zero reflections and transmissions. The following points are observed from the results in Figs. 8(a) and 8(b). First, extracted and reference values ($\varepsilon_r = 3.48(1 - j0.0037)$[33] and $\varepsilon_r = 4.3(1 - j0.025)$[35]) of ε_r' and tanδ of the tested Rogers 4350B and FR-4 samples are in good agreement over the entire frequency band. Second, retrieved ε_r' and tanδ of both samples for the NZR-1 and NZR-2 cases have lower oscillatory behavior (ripples) than those for the zero reflection case (ZR case). Such an oscillatory behavior is chiefly associated with disparity at antenna regions and non-negligible reflections (ringing effect) between antennas and each sample. Third, this ringing effect produce tanδ values lower than zero (non-physical) at some frequencies (e.g., 10.72 GHz) for the tested Rogers 4350B sample for the zero reflection case (ZR case).

Inline with our recent study[21], the performances of the aforementioned three different cases (ZR, NZR-1, and NZR-2) were examined using quantitative error estimates (using five independent measurements). Tables 2 and 3 give evaluated ε_r and tanδ of the Rogers 4350B and FR-4 samples at $f = 8.2$ GHz (the minimum frequency), 10.3 GHz (the mid-frequency), and 12.4 GHz (the maximum frequency) frequencies for all three cases after utilizing the GUM-uncertainty model analyzed in[21] ($\Delta|F_{\text{obj}}| = 0.05$, $\Delta\theta_{\text{obj}} = 1^o$, and $\Delta W = 0.01$ mm). The following three main deductions can be inferred from the results in Tables 2 and 3. First, retrieved ε_r has lower percentage variations than δ has for either sample mainly due to low-loss nature of tested samples and reduced accuracy of non-resonant methods for low-loss samples. Second, the NZR-1 and NZR-2 cases have comparatively lower ε_r and tanδ percentage variations than the ZR case for both tested samples at all discrete frequencies. We think that this is the composite effects of disparity at antenna regions and non-negligible reflections (ringing effect) between antennas and each sample. Third, the NZR-1 and NZR-2 cases have close percentage variations for ε_r and tanδ for both samples at all discrete frequencies. This is because NZR-1 and NZR-2 cases utilize the same objective function F_{obj} in (23). Nonetheless, the free-space model in Fig. 1 is more general that those considered in the studies[16,19,21], suitable for applications involving a free-space measurement setup having two different transmitting and receiving antenna regions (e.g., $[T] \neq [R]$).

ARTICLE IN PRESS

6 Advantages and Limitations of Our Method

A general free-space model considering the case that $[T] \neq [R]$ is examined in the present study. An objective function based on this model and specialized for electrically thinner samples is derived with no requirement of any formal calibration procedure such as the TRL method, unlike previous extraction methods in the literature[4–13,15,17,19,21,22]. Additionally, our extraction method uses both reflection and transmission measurements, providing more information at one frequency than other reflection-only methods[14,18,20]. Nonetheless, our method requires reflection measurements along with transmission measurements, which are not feasible for applications where the other side of the sample is not accessible. As the second drawback, the samples are assumed to be free-standing with no support by any sample holder. This means that for extremely thinner samples, the sample sagging[5] plays a critical role for limiting the accuracy of the proposed method due to non-uniform sample surface pattern. As another limitation, precise sample thickness needs to be provided for improved ε_r determination by the proposed method. As the final drawback of our method, angle misalignment lowers the accuracy of our method, as considered in Section 4. Thus, a proper sample alignment in reference with antenna apertures is a critical factor for accurate ε_r determination by the proposed method.

On the other hand, it is instructive to discuss that the objective function F_{obj} in (23) is valid for thinner ($W < \lambda/4$) or thicker ($W > \lambda/4$) dielectric samples with low-loss, medium-loss, or high-loss behavior, since there was not any assumption enforced over it in its derivation procedure. Nevertheless, the objective functions G_{obj} in (24) and H_{obj} in (25) are strictly applicable for thinner low-loss dielectric samples only because $\sinh(b\phi_0) \approx b\phi_0$ and $\cosh(b\phi_0) \approx 1.0$ assumptions were exercised in their derivations. In other words, if a thicker low-loss (medium-loss or high-loss) dielectric sample is being characterized, then F_{obj} could be directly utilized to determine ε_r. However, it is noteworthy that F_{obj} then necessitates a good initial guess ε_r for a thicker low-loss (medium-loss or high-loss) dielectric sample, because $\cos[(1-\sqrt{\varepsilon_r})k_0W]$ and $\cos[(1+\sqrt{\varepsilon_r})k_0W]$ terms are multi-valued terms. Finally, it is noted that all the objective functions (F_{obj}, G_{obj}, and H_{obj}) derived in this present study assume that the sample under examination is a dielectric sample. The terms Γ and T in (21) could be generalized to reflect magnetic behavior of a general (magnetic) sample:

$$\Gamma = \frac{\sqrt{\frac{\mu_r}{\varepsilon_r}} - 1}{\sqrt{\frac{\mu_r}{\varepsilon_r}} + 1} \tag{27}$$

$$T = e^{-jk_0\sqrt{\mu_r\varepsilon_r}W}, \tag{28}$$

where μ_r is the magnetic permeability of the sample. Since, then, there is one complex (real and imaginary parts) measurement data but two complex unknowns (ε_r and μ_r), the system turns into an underdetermined system, meaning there are fewer equations (constraints) than unknowns (variables) with infinitely many solutions rather than a single unique solution. For this reason, we constrained our analysis to dielectric samples only in the present study. In future, our goal is to determine unique solution for both ε_r and μ_r considering an additional measurement or additional measurements.

7 Conclusion

A theoretical model generalizing the configuration of a free-space measurement environment is considered in this study. Distinct from previous free-space models, the proposed model takes into account of different error network models for transmitting and receiving antennas with non-zero and non-identical reflection and transmission properties. Such a model applicable for any frequency or over the entire frequency band examines different antenna characteristics involving impedance mismatches and ringing effects between antennas and the sample. An objective function is derived for ε_r retrieval of low-loss and electrically thin samples based upon this generalized model, with the advantages of non-dependence on error network elements and reference plane transformation factors. From the analysis of angle misalignment effect, it is noted that the proposed method requires precise sample alignment to improve the accuracy of ε_r evaluation. Free-space measurements of ε_r of two low-loss and electrically thin samples (the Rogers 4350B sample with $W \approx 1.52$ mm and the FR-4 sample with $W \approx 1.60$ mm) are performed to validate and evaluate the performance of the proposed method.

References

1. Filbert, J. T., Dvorsky, M. R., Tayeb Al Qaseer, M. & Zoughi, R. Unambiguous determination of complex dielectric and magnetic materials properties using multilength nicolson-ross–weir approach. *IEEE Transactions on Instrumentation Meas.* **74**, 1–12, DOI: 10.1109/TIM.2025.3544726 (2025).

ARTICLE IN PRESS

2. Kharkovsky, S. & Zoughi, R. Microwave and millimeter wave nondestructive testing and evaluation - overview and recent advances. *IEEE Instrumentation & Meas. Mag.* **10**, 26–38, DOI: 10.1109/MIM.2007.364985 (2007).

3. Brinker, K., Dvorsky, M., Al Qaseer, M. T. & Zoughi, R. Review of advances in microwave and millimetre-wave ndt&e: principles and applications. *Philos. Transactions Royal Soc. A: Math. Phys. Eng. Sci.* **378**, 20190585, DOI: 10.1098/rsta.2019.0585 (2020). https://royalsocietypublishing.org/doi/pdf/10.1098/rsta.2019.0585.

4. Ghodgaonkar, D., Varadan, V. & Varadan, V. A free-space method for measurement of dielectric constants and loss tangents at microwave frequencies. *IEEE Trans. Instrum. Meas.* **38**, 789–793 (1989).

5. Ghodgaonkar, D. K., Varadan, V. V. & Varadan, V. K. Free–space measurement of complex permittivity and complex permeability of magnetic materials at microwave frequencies. *IEEE Trans. Instrum. Meas.* **39**, 387–394 (1990).

6. Varadan, V., Hollinger, R., Ghodgaonkar, D. & Varadan, V. Free-space, broadband measurements of high-temperature, complex dielectric properties at microwave frequencies. *IEEE Trans. Instrum. Meas.* **40**, 842–846 (1991).

7. Rashidian, A., Shafai, L., Klymyshyn, D. & Shafai, C. A fast and efficient free-space dielectric measurement technique at mm-wave frequencies. *IEEE Antennas Wirel. Propag. Lett.* **16**, 2630–2633 (2017).

8. Yang, C., Ma, K. & Ma, J.-G. A noniterative and efficient technique to extract complex permittivity of low-loss dielectric materials at terahertz frequencies. *IEEE Antennas Wirel. Propag. Lett.* **18**, 1971–1975 (2019).

9. Zhou, K. *et al.* Dielectric constant and loss tangent of silicon at 700–900 ghz at cryogenic temperatures. *IEEE Microw. Wirel. Components Lett.* **29**, 501–503, DOI: 10.1109/LMWC.2019.2920532 (2019).

10. Hasar, U. C., Ozturk, G., Bute, M. & Ertugrul, M. Method for electromagnetic property extraction of sublayers in metal-backed inhomogeneous metamaterials. *IEEE Access* **8**, 151705–151718, DOI: 10.1109/ACCESS.2020.3007579 (2020).

11. Hasar, U. C. *et al.* Feasible extraction method for electromagnetic properties of multilayer metamaterials with short-circuit termination. *IEEE Transactions on Antennas Propag.* **70**, 10650–10659, DOI: 10.1109/TAP.2022.3195500 (2022).

12. Andrushchak, N. A. *et al.* New interference technique for determination of low loss material permittivity in the extremely high frequency range. *IEEE Transactions on Instrumentation Meas.* **64**, 3005–3012, DOI: 10.1109/TIM.2015.2437631 (2015).

13. Kim, S., Novotny, D., Gordon, J. A. & Guerrieri, J. R. A free-space measurement method for the low-loss dielectric characterization without prior need for sample thickness data. *IEEE Trans. Antennas Propag.* **64**, 3869–3879 (2016).

14. Li, L. *et al.* Compact dielectric constant characterization of low-loss thin dielectric slabs with microwave reflection measurement. *IEEE Antennas Wirel. Propag. Lett.* **17**, 575–578 (2018).

15. Yashchyshyn, Y. & Godziszewski, K. A new method for dielectric characterization in sub-thz frequency range. *IEEE Transactions on Terahertz Sci. Technol.* **8**, 19–26 (2018).

16. Zhu, H.-T. & Wu, K. Complex permittivity measurement of dielectric substrate in sub-thz range. *IEEE Trans THz Sci. Technol.* **11**, 2–15 (2021).

17. Cao, B., Wang, M., Li, X., Fan, M. & Tian, G. Noncontact thickness measurement of multilayer coatings on metallic substrate using pulsed terahertz technology. *IEEE Sensors J.* **20**, 3162–3171, DOI: 10.1109/JSEN.2019.2958674 (2020).

18. Hasar, U. C., Kaya, Y., Oztuk, G., Ertugrul, M. & Korasli, C. Broadband, stable, and non-iterative dielectric constant measurement of dielectric slabs using an effective frequency-domain free-space method. *IEEE Trans. Antennas Propag.* **70**, 12435–12439 (2022).

19. Xue, B. Characterizing complex permittivity of thin materials by free-space transmission and reflection coefficients. *IEEE Antennas Wirel. Propag. Lett.* **23**, 4438–4442, DOI: 10.1109/LAWP.2024.3450634 (2024).

20. Xue, B., Haneda, K., Icheln, C., Ala-Laurinaho, J. & Tuomela, J. Complex permittivity characterization of low-loss dielectric slabs at sub-thz. *IEEE Access* **12**, 150693–150701, DOI: 10.1109/ACCESS.2024.3479908 (2024).

21. Hasar, U. C., Korkmaz, H. & Kaya, Y. Electromagnetic characterization of electrically thin low-loss materials through uncalibrated frequency-domain free-space measurements. *IEEE Transactions on Antennas Propag.* (2026 (Under revision)).

22. Sun, F., Cao, B., Fan, M., Ye, B. & Pan, J. Physics-constrained transfer learning for self-assessment of terahertz thickness measurement of thermal barrier coatings. *IEEE Transactions on Ind. Informatics* **20**, 11045–11056, DOI: 10.1109/TII.2024.3400318 (2024).

23. Frolik, J. Reconstruction of multilayered lossy dielectrics from one-sided plane wave impulse reflection responses: the bistatic case. *IEEE Trans. Geosci. Remote. Sens.* **39**, 2051–2059 (2001).

ARTICLE IN PRESS

ARTICLE IN PRESS

24. Caorsi, S. & Stasolla, M. A layer stripping approach for em reconstruction of stratified media. *IEEE Transactions on Geosci. Remote. Sens.* **52**, 5855–5869, DOI: 10.1109/TGRS.2013.2293533 (2014).

25. Akhter, Z. & Akhtar, M. J. Free-space time domain position insensitive technique for simultaneous measurement of complex permittivity and thickness of lossy dielectric samples. *IEEE Trans. Instrum. Meas.* **65**, 2394–2405 (2016).

26. Akhter, Z., Jha, A. K. & Akhtar, M. J. Generalized rf time-domain imaging technique for moving objects on conveyor belts in real time. *IEEE Trans. Microw. Theory Techn.* **65**, 2536–2546 (2017).

27. Xue, B., Tuomela, J., Haneda, K., Icheln, C. & Ala-Laurinaho, J. Permittivity characterization of human skin at sub-thz using free space reflection coefficients. *IEEE Transactions on Microw. Theory Tech.* **73**, 2752–2765 (2025).

28. Huang, Z. *et al.* Dual-band air-like transparent slab by full polarization compensation. *IEEE Transactions on Antennas Propag.* **72**, 8762–8771, DOI: 10.1109/TAP.2024.3464859 (2024).

29. Hasar, U. C., Kaya, Y., Korkmaz, H. & Iliev, T. Broadband multilayer absorber design using double-stage cognitive seeker optimization algorithm. *IEEE Access* **13**, 27178–27190, DOI: 10.1109/ACCESS.2025.3537661 (2025).

30. Baker-Jarvis, J., Vanzura, E. J. & Kissick, W. A. Improved technique for determining complex permittivity with the transmission/reflection method. *IEEE Trans. Microw. Theory Techn.* **38**, 1096–1103 (1990).

31. Pozar, D. M. *Microwave Engineering* (Wiley, West Sussex, England, 2011).

32. Fu, Y., Savkin, A. V., Yuk Chan, K. & Ramer, R. Resolving ambiguity in permittivity extraction by noniterative method with less dependence on calibration. *IEEE Transactions on Microw. Theory Tech.* 1–12, DOI: 10.1109/TMTT.2025.3639092 (2025).

33. Corporation, R. https://rogerscorp.com/-/media/project/rogerscorp/documents/advanced-electronics-solutions/english/data-sheets/ro4000-laminates-ro4003c-and-ro4350b—data-sheet.pdf. (2022).

34. 100:2008, J. Evaluation of measurement data — guide to the expression of uncertainty in measurement (gum 1995 with minor corrections).

35. Djordjevic, A., Biljie, R., Likar-Smiljanic, V. & Sarkar, T. Wideband frequency-domain characterization of fr-4 and time-domain causality. *IEEE Transactions on Electromagn. Compat.* **43**, 662–667, DOI: 10.1109/15.974647 (2001).

Acknowledgements

Authors would like to thank the Scientific Research Unit of Gaziantep University (Türkiye) for providing grants to our laboratory (Applied Electromagnetics Research Laboratory (Aer-Lab) - https://aer-lab.gantep.edu.tr) to support our research activities.

Data availability

The datasets used and analyzed during the current study are available from the corresponding author (U.C.H) upon reasonable request.

Author contributions statement

U.C.H. and H.K. investigated the subject; U.C.H., H.K., and Y.K. performed conceptualization analysis; U.C.H. and H.K. conducted the experiments; U.C.H. and H.K. validated the results; U.C.H., H.K., and Y.K. prepared illustrations (visualization); U.C.H., H.K., and Y.K. analyzed the results; U.C.H. and Y.K. prepared the original draft; and U.C.H. supervised the study.

Competing interests

The authors declare no competing interests.

Funding

There is no specific funding.

ARTICLE IN PRESS